# Vibrational modes in $ZnGeN_2$: Raman study and theory

Timothy J. Peshek, Tula R. Paudel, Kathleen Kash, and Walter R. L. Lambrecht
*Department of Physics, Case Western Reserve University, Cleveland, Ohio 44106-7079, USA*
(Received 3 March 2008; published 23 June 2008)

Polarized Raman spectra were measured for single crystals and polycrystalline $ZnGeN_2$ grown by a vapor-liquid-solid method. A group-theoretical analysis of the selection rules governing the predicted dependence of the spectra on incoming and outgoing wave polarizations and propagation direction is presented. First-order Raman spectra corresponding to the zone center phonons are calculated from first principles using density functional perturbation theory. The Brillouin zone integrated density of phonon states is also calculated. Comparison of theory and experiment allows us to identify the $a_{1t}$ symmetry modes. However, vibrational density of states features deviating from the pure $a_{1t}$ spectrum are also visible in the experimental spectra and indicate some relaxation of momentum conservation rules. Differences in the experimental spectra under different polarization conditions are compared to the calculations. These differences allow us to identify different $a_{1t}$ Raman tensor components as well as to obtain at least partial information on the $b_{2t}$ modes. The much weaker polarization dependence in experiment than in theory, however, can at least in part be explained by using wurtzite-type selection rules. The observation of features explainable with wurtzite together with orthorhombic selection rules suggest that there is only partial ordering of the cations on their sublattice.

DOI: 10.1103/PhysRevB.77.235213 PACS number(s): 78.30.Fs, 63.20.dk

## I. INTRODUCTION

$ZnGeN_2$ is a close cousin to GaN. Its crystal structure is closely related to wurtzite and has locally each N coordinated by two Ge and two Zn instead of four Ga. These atoms being close in mass and valence charge, one might expect very similar electronic band structure as well as vibrational spectra. Because of the enlarged unit cell related to the ordering of the Ge and Zn, one might expect a zone folding picture to hold and thus to obtain additional information on modes that in wurtzite would lie at the zone boundary. Yet, a previous computational study[1] showed that the bimodal bond-length distribution, Zn-N bonds being longer than Ge-N bonds, leads to a quite different phonon spectrum from that of GaN. The only previous experimental study of the phonons in this material was a Raman study on polycrystalline powder samples.[2] Because of the size of the unit cell (16 atoms), there are many closely spaced modes. Without selection rules offered by polarized Raman spectroscopy on well oriented single crystals, it is nearly impossible to unravel these modes. In fact, all modes are Raman active in this structure. Compared to wurtzite GaN with only six Raman active modes (counting LO and TO modes of the same symmetry separately), $ZnGeN_2$ has 78 Raman active modes. The previous theoretical study discussed the experimental spectra in terms of a density-of-states-like superposition of all the modes at $\Gamma$ and also found evidence for second-order Raman features, e.g., high frequency peaks were tentatively assigned to two-phonon scattering or second harmonics. Some uncertainties concerning the structure may play a role. While the orthorhombic crystal structure arises from a well-defined ordering of the Zn and Ge on the hexagonally close packed cation sublattice, accompanied by slight distortions, it is difficult to observe this ordering directly by x-ray diffraction because of the closeness in electron density of the Zn and Ge ions. In fact, this ordering has only been observed by neutron diffraction.[3] Previous studies had labeled the structure as monoclinic but very close to hexagonal.[4] For details on the relationships of these various crystal structures, see Ref. 1. The question arises whether Raman spectroscopy is sensitive to the ordering of the cations.

Here, we present a Raman study of small single crystals of $ZnGeN_2$, 3–4 $\mu$m in diameter, 30–40 $\mu$m in length with hexagonal cross sections, as well as polycrystalline material. They were grown by a different approach than used in the previous Raman study. The growth method is discussed briefly in Sec. II and is fully described in Refs. 5 and 6. Polarized Raman spectra in various geometries were measured using a micro-Raman spectrometer, as detailed in Sec. II. Group theory is used to analyze the selection rules applicable for each geometry (Sec. III). Our previous computational study is extended by calculating quantitatively the Raman intensities using density functional perturbation theory and by calculating the full Brillouin zone integrated density of states, as described in Sec. VI. A direct comparison of the experimental and calculated spectra is presented in Sec. V. We focus here primarily on the $a_{1t}$ mode, which as we shall show is predicted to give by far the largest intensities and is the mode measured when incoming and outgoing light have the same polarization. Good agreement is obtained with the measurements in this geometry. Almost all expected individual modes are identified in the experimental spectrum. Some additional features observed appear to be related to the density of phonon states and thus indicate a relaxation of momentum conservation rules. In any case, the measured spectra are quite different from the previous spectra on powders in the literature[2] and do not show the high frequency harmonics. We also present spectra measured on our own polycrystalline material. The polarization dependence of the spectra is discussed and provides partial information on other symmetry modes. However, the weaker signals for these other modes are difficult to extract for reasons noted below. The relation of the spectra to the dominant modes in wurtzite Raman spectra is discussed. The fact that all the $a_{1t}$ modes predicted by theory could be identified in the spectra pro-

 

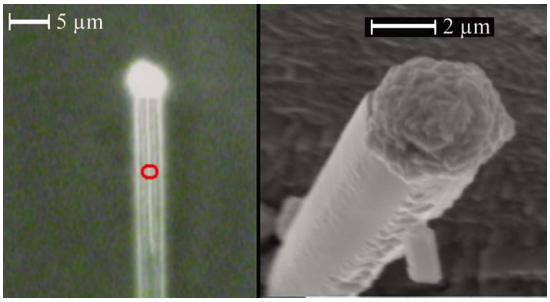


FIG. 1. (Color online) $ZnGeN_2$ single crystal needle; left: optical micrograph, right: scanning electron microscopy image of a similar needle, showing the polycrystalline dome at the end. The red circle marks the spot size and location for the Raman measurement. Although not apparent in the left image, there is a facet oriented with its normal to the plane of the image.

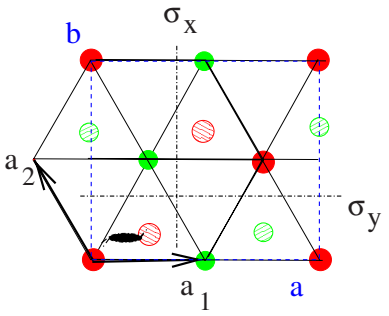


FIG. 2. (Color online) Crystal structure of $ZnGeN_2$ and its relation to the wurtzite structure. The large solidly filled red spheres represent Ge atoms in the basal plane, the red shaded spheres Ge atoms in a plane at height $c/2$, the smaller solidly filled green spheres represent Zn atoms in the basal plane, and the green shaded spheres represent Zn atoms at height $c/2$. $N_1$ atoms sit almost directly above Ge and $N_2$ atoms directly above Zn atoms. Glide mirror planes are indicated by the dashed-dotted lines and the screw axis by the ellipse.

vides clear evidence of ordering of the cations. However, the imperfect suppression of some peaks upon changing the polarization indicates that this ordering is not perfect. A summary of the main results concludes the paper (Sec. IV).

## II. EXPERIMENTAL APPROACH

The samples were grown by a vapor-liquid-solid method that employed high purity Zn and Ge loaded into a graphite crucible and exposed to 30 mbar $NH_3$ at 750 °C in a quartz tube reactor for 16 h.[6] Hexagonally faceted single crystal rods, approximately 3–4 $\mu$m in width, 30–50 $\mu$m in length, and capped with hemispherical domes, as well as polycrystalline flakes, formed during the growth. Electron diffraction and energy dispersive x-ray analysis on a single faceted rod confirmed that the rod is single crystal $ZnGeN_2$ and the dome is polycrystalline $ZnGeN_2$.[6] Scanning electron microscopy images of the polycrystalline domes indicate that they are composed of randomly oriented crystallites of dimensions of the order of 0.1–0.1–1 $\mu$m.

The crystallites were separated after growth from the remaining Ge-Zn alloy by etching first in a 50% $HNO_3$:$H_2O$ solution to remove excess Zn, then in a 30% $H_2O_2$:$H_2O$ solution to remove excess Ge. Samples were prepared for Raman spectroscopy by diluting the etchant with distilled water, centrifuging, and dispersing droplets of solution onto glass slides.

Polarized Raman spectra were acquired on a Jobin Yvon LabRam HR 800 Raman microscope using the 632 nm wavelength line of a He-Ne laser and a focused spot size diameter of approximately 2 $\mu$m. Sample orientations were aligned relative to the incident polarization direction with an estimated uncertainty of ±2°. A polarization rotator was used at the exit of the spectrometer to align the polarization of the scattered light along the axis of the spectrometer's diffraction grating, independent of the choice of scattered light polarization, thus maintaining the same detection sensitivity for different scattered polarizations and therefore allowing for comparison of the spectra on an absolute scale. The uncertainty in the reported wave number is ±2 $cm^{-1}$. Figure 1 shows an optical and scanning electron microscopy image of one of the needle-shaped crystals showing the dome at the end. The red circle marks the spot size and location of the laser beam for the Raman measurements on the single crystal.

## III. CRYSTAL STRUCTURE AND SELECTION RULES

The crystal structure is a $2\times2\times1$ superlattice of the wurtzite structure. The correspondence between the primitive vectors of the orthorhombic and wurtzite unit cells is chosen as follows:

$$\mathbf{a}^o = 2\mathbf{a}_1^h, \quad \mathbf{b}^o = \mathbf{a}_1^h + 2\mathbf{a}_2^h, \quad \mathbf{c}^o = \mathbf{c}^h. \tag{1}$$

This **b** axis is sometimes referred to as the orthohexagonal axis. The experimental values reported by Wintenberger *et al.*[3] but reordered in our notation, with $a$ to $c$ from highest to lowest values, are $a$=6.441 Å, $b$=5.454 Å, and $c$ =5.194 Å.

Slight distortions occur from the ideal hexagonal structure. While without distortion $b$ would be $\sqrt{3}a^h$=1.732$a^h$, with distortion it is compressed by 2.3% to 1.693$a_h$. The $c/a^h$ ratio is 1.613 compared to 1.626 in GaN. Referring to Fig. 2, it implies that the hexagons in the bond network are now slightly irregular with a long side, $|\mathbf{a}_1^h|=a^o/2$ =3.2205 Å, and a short side, $\mathbf{a}_2^h=\sqrt{(a^o/4)^2+(b^o/2)^2}$ =3.1669 Å, and the angles are no longer 120°. The angle between $\mathbf{a}_1$ and $\mathbf{a}_2$ is 120°33′ and the angle between two short sides is 118°53′. The Ge and Zn atoms are placed, respectively, at (0,0,0) and (1/2,0,0) (and equivalent positions by symmetry) with the $N_1$ and $N_2$ almost directly on top of them at about 0.375$c$ but slightly displaced such that the N atoms move closer to the two Ge and away from the two Zn surrounding them.[1] Crystallites may be expected to exhibit either $(10\bar{1}0)$ facets or $(11\bar{2}0)$ facet. In the former case, the hexagons bounding the crystal are oriented exactly as the hexagons in the bonding network seen in Fig. 2. In the latter case, they are rotated by 30°.

The space group is $Pna2_1$. The symmetry elements indicated in Fig. 2 are a twofold screw axis passing through the

TABLE I. Character table for the group $C_{2v}$, first column; basis functions, second column; irreducible representations, first row; and classes.

| | | $E$ | $C_{2z}$ | $\sigma_x$ | $\sigma_y$ |
|---|---|---|---|---|---|
| $z$ | $a_1$ | 1 | 1 | 1 | 1 |
| $x$ | $b_1$ | 1 | −1 | −1 | 1 |
| $y$ | $b_2$ | 1 | −1 | 1 | −1 |
| | $a_2$ | 1 | 1 | −1 | −1 |

point (1/8,1/6) in reduced coordinates (i.e., in units $a$ and $b$), including a shift along $c$ by $(1/2)c$; a glide mirror-plane perpendicular to the **a** axis passing through $-(1/8)\mathbf{a}$ and involving a shift parallel to the plane by $\mathbf{b}/2$; a glide plane perpendicular to the **b** axis passing at 1/3 of the $b$ axis and involving a shift by $\mathbf{a}/2$ and $\mathbf{c}/2$. Only one of the equivalent symmetry operations located at other points in the cell is shown for each type. These are denoted as $\{C_{2z}|(\frac{1}{4},\frac{1}{6},\frac{1}{2})\}$, $\{\sigma_x|(-\frac{1}{4},\frac{1}{2},0)\}$, and $\{\sigma_y|(\frac{1}{2},-\frac{1}{3},\frac{1}{2})\}$, respectively. The point group is $C_{2v}$. The character table is given in Table I.

In first-order Raman spectroscopy, only phonon modes at $\Gamma$ are allowed because of the requirement for momentum conservation and the negligible momentum of the photon. Thus, the point group symmetry group $C_{2v}$ is applicable. All modes are Raman active. The 16 atoms in the unit cell correspond to 48 degrees of freedom. They give rise to 12 modes of each irreducible representation. One each of the $a_1$, $b_1$, and $b_2$ modes corresponds to a pure translation along $z$, $x$, or $y$, respectively, and thus has zero frequency. There remain 45 modes. However, the 11 $a_1$, $b_1$ and $b_2$ modes each experience a transverse-longitudinal splitting so that one expects a total of 78 modes. The calculated frequencies of these modes were reported by Lambrecht *et al.*[1]

The Raman scattering cross section for a Stokes process in which light with incoming angular frequency $\omega_0$ and polarization $\mathbf{e}_i$ is scattered into light with frequency $(\omega_0-\omega_n)$ and polarization $\mathbf{e}_o$ is given by[7]

$$\frac{dS}{d\Omega}=|\mathbf{e}_i\cdot\mathcal{R}^m\cdot\mathbf{e}_o|^2=\frac{(\omega_0-\omega_n)^4}{c^4}|\mathbf{e}_i\cdot\alpha^m\cdot\mathbf{e}_o|^2\frac{\hbar}{2\omega_n}(n_m+1), \tag{2}$$

where $\omega_n$ is the phonon frequency of mode $m$, $n_m$ is the thermal occupation number of that phonon mode, i.e., the boson factor, and $\mathcal{R}^m$ is the second order Raman tensor. The Raman susceptibility tensor $\boldsymbol{\alpha}^m$ is given by

$$\alpha^m_{\alpha\beta}=\sqrt{V}\sum_{\kappa\gamma}\frac{\partial\chi_{\alpha\beta}}{\partial\tau_{\kappa\gamma}}u_m(\kappa\gamma), \tag{3}$$

where $V$ is the volume of the unit cell, $\chi_{\alpha\beta}$ is the first-order dielectric susceptibility tensor, $\tau_{\kappa\gamma}$ is the Cartesian coordinate in direction $\gamma$ of atom $\kappa$ in the unit cell, and $u_m(\kappa\gamma)$ is the eigenvector corresponding to mode $m$. The quantities $d\chi_{\alpha\beta}/d\tau_{\kappa\gamma}$ form a third rank tensor. By taking the dot product of this tensor with the displacement components of each atom for a given mode, we obtain a second rank tensor. Clearly, in order to have a nonzero $\alpha^m_{\alpha\beta}$ contribution, the direct product of the irreducible representations corresponding to $\alpha$ and $\beta$ must contain the irreducible representation of the mode $m$. Using the character table, we can see that for $a_1$ modes, we must have $\alpha=\beta$ so the Raman tensor has only diagonal components. Still, because of the orthorhombic symmetry, this tensor has three different diagonal components. Thus, for $a_{1t}$ symmetry modes, we have a Raman tensor of the form

$$\begin{pmatrix} a^{1t}_{xx} & & \\ & a^{1t}_{yy} & \\ & & a^{1t}_{zz} \end{pmatrix}. \tag{4}$$

Using the notation $\mathbf{k}_i(\mathbf{e}_i,\mathbf{e}_o)\mathbf{k}_o$ for the geometry corresponding to incoming (outgoing) light wave vectors $\mathbf{k}_i$ and $\mathbf{k}_o$ and polarizations $\mathbf{e}_i$ and $\mathbf{e}_o$, we can see that the $a^1_{zz}$ component will be measured by a scattering geometry $x(zz)\bar{x}$ or $y(zz)\bar{y}$. Here, $\bar{x}=-x$ indicates reflection geometry. Since in both cases the wave vector is perpendicular to $z$, which corresponds to $a_1$, the modes visible in this geometry are transverse. So, this component of the $a_{1t}$ spectrum is measured when the incoming and scattered light are both polarized along the $c$ axis of the crystal and the wave vector is perpendicular to the $c$ axis. The $a^{1t}_{xx}$ component will be obtained in a scattering geometry $y(xx)\bar{y}$ and $a^{1t}_{yy}$ in a scattering geometry $x(yy)\bar{x}$. All of these will be easiest to perform on needle-type crystals with their long axes oriented along $c$ and lying flat on the glass holder. The corresponding longitudinal spectrum could be measured in the geometry $z(xx)\bar{z}$ giving the $a^{1l}_{xx}$ component of the Raman tensor and $z(yy)\bar{z}$ giving $a^{1l}_{yy}$. This measurement would be easiest on (0001)-oriented platelet crystallites or (0001)-oriented films. The $a^{1l}_{zz}$ component cannot be measured because it would require $z(zz)\bar{z}$, which is obviously impossible. It should be pointed out here that because of the relatively low symmetry, the vibrational motions are generally not purely longitudinal or transverse in the sense of being parallel or perpendicular to the wave vector, but have a mixed character. However, $a_1$ symmetry modes can couple to electric fields along the $z$ axis. For a wave vector $\mathbf{q}$ along $z$, Gauss's law $\mathbf{q}\cdot\mathbf{D}=0$ requires that $\varepsilon(\omega)=0$, and in this sense, we have a longitudinal mode. On the other hand, if $\mathbf{q}\perp\mathbf{c}$, then $\mathbf{q}\times\mathbf{E}=0$ requires that $\varepsilon^{-1}(\omega)=0$; in other words, one obtains poles of the dielectric function, or transverse optical modes.

Because $a_1\otimes b_1=b_1$, the only nonzero component of the Raman tensor corresponding to $b_1$ modes is clearly the $xz$ component. So, the tensor is of the form

TABLE II. Scattering geometry, corresponding nonzero Raman tensor component, and preferred crystallites.

| $\mathbf{k}_i(\mathbf{e}_i\mathbf{e}_o)\mathbf{k}_o$ | $\mathcal{R}^m_{\alpha\beta}$ | Crystal shape |
|---|---|---|
| $y(zz)\bar{y}$ | $a^{1t}_{zz}$ | Needle |
| $x(zz)\bar{x}$ | $a^{1t}_{zz}$ | Needle |
| $x(yy)\bar{x}$ | $a^{1t}_{yy}$ | Needle |
| $y(xx)\bar{y}$ | $a^{1t}_{xx}$ | Needle |
| $z(xx)\bar{z}$ | $a^{1l}_{xx}$ | Platelet |
| $z(yy)\bar{z}$ | $a^{1l}_{yy}$ | Platelet |
| $x(yz)\bar{x}$ | $b^{2t}_{yz}$ | Needle |
| $y(xz)\bar{y}$ | $b^{1t}_{xz}$ | Needle |
| $z(xy)\bar{z}$ | $a^{2}_{xy}$ | Platelet |

$$\begin{pmatrix} & & b_1 \\ & 0 & \\ b_1 & & \end{pmatrix} \tag{5}$$

and is measured by a process $y(zx)\bar{y}$ or $y(xz)\bar{y}$. Because the propagation direction $y$ is perpendicular to the mode direction $b_1=x$, we measure the transverse component. So, this requires measuring the incoming and outgoing light with perpendicular polarizations but can again be done on flat-lying needle-shaped crystals if they lie with their $x$ axis in the plane of the holder. Similarly, $b_{2t}$ modes can be measured in a geometry $x(yz)\bar{x}$. The longitudinal modes $b_{1l}$ and $b_{2l}$ cannot be measured by Raman scattering.

Finally, because $b_1 \otimes b_2 = a_2$, the Raman tensor for the $a_2$ modes only has $xy$ components. Thus, we would measure these modes in the $z(xy)\bar{z}$ geometry on platelet crystals with their $c$ axes perpendicular to the plane.

In summary, ideally, it should be possible to measure the three different diagonal components of the $a^{1t}$ Raman tensor and the the $b_{1t}$ and $b_{2t}$ modes, which each have only one nonzero Raman tensor component, by polarized Raman spectroscopy on needle-shaped crystals, and the $a_2$ modes and $a^{1l}_x$ and $a^{1l}_y$ components on platelet crystals, as summarized in Table II. In practice, it is not so easy to determine the actual alignment of the crystallites. While it is easy to see the $c$ axis, it is difficult to determine whether the crystals lie down with their $a$ axis or with their $b$ axis parallel to the glass slide or at a 30° angle. The orientation depends on two factors: (1) which are the habit planes of the crystal, $(10\bar{1}0)$ or $(11\bar{2}0)$, and (2) which particular plane is lying face down, the long side of the hexagon or the short side (see the discussion above). The deviations from a perfect hexagon are too small to detect visually. Possibly, the Raman spectra themselves can reveal how the crystallites are oriented by comparison to the calculated spectra. Furthermore, as we will see from the quantitative calculations, the $a_1$ Raman tensor components are approximately an order of magnitude stronger than the other components.

It is of interest to relate the symmetries of the vibrational modes in the orthorhombic structure to the modes in their parent hexagonal wurtzite structure. In wurtzite, there are two $B_1$ modes (silent), two $E_2$ modes (only Raman active), one $A_1$ mode, and one $E_1$ mode (the last two are both infrared and Raman active and thus split into longitudinal and transverse modes), corresponding to the point group $C_{6v}$. We will indicate these modes here by capital letters so as not to confuse them with the modes for the $C_{2v}$ group. The upper $E_2$ mode is one in which only the lighter N atoms are moving, and the cations are stationary. When lowering the symmetry from $C_{6v}$ to $C_{2v}$ we have the following compatibilities: $A_1 \rightarrow a_1$, $B_1 \rightarrow b_1$, $E_1 \rightarrow b_1 \oplus b_2$, and $E_2 \rightarrow a_1 \oplus a_2$. Thus, the silent modes of wurtzite become allowed in the orthorhombic system but are still expected to be weak. The stronger $b_1$ and $b_2$ modes are thus expected to arise from the splitting of the parent $E_1$-like modes. The scattering geometry $y(xx)\bar{y}$ or $x(yy)\bar{x}$ allows one to see $A_{1t}$ and $E_2$ modes in wurtzite and the scattering geometry $x(zz)\bar{x}$ would give only $A_{1t}$ modes. The strongest mode typically seen in a wurtzite GaN $y(xx)\bar{y}$ spectrum is the $E_2$-high mode. This mode has a Raman tensor of the form

$$\begin{pmatrix} d & d & 0 \\ d & -d & 0 \\ 0 & 0 & 0 \end{pmatrix} \tag{6}$$

and is thus active both with parallel and perpendicular incoming and scattered light polarizations as long as both polarizations are perpendicular to the $c$ axis.

## IV. COMPUTATIONAL METHOD

The computational method for calculating the vibrational modes is the same as in Refs. 1 and 8. In short, we use density functional calculations[9,10] in the local density approximation,[11] with norm-conserving pseudopotentials as generated by workers at the Fritz–Haber institute[12] and a plane wave basis set as implemented in ABINIT.[13] The plane wave cutoff is set at 80 Ry and a $4\times4\times4$ **k**-point mesh is used to sample the Brillouin zone in the self-consistent calculations. The crystal structure is first relaxed with respect to the atomic coordinates and the lattice parameters and gives excellent agreement with experimental values.[1] The vibrational modes at the zone center are calculated using the linear response technique,[14] which is based on density functional perturbation theory and implemented in terms of a conjugate gradient minimization approach following Gonze and co-workers.[15,16] The longitudinal-optical splittings in this approach are included by calculating the response to static electric fields as well as to the atomic displacements. The symmetries of the modes are determined by inspection of the eigenvectors. In this paper, we also calculate the density of phonon states integrated over the Brillouin zone. To do this, the force constants are separated into long-range and short range parts for a coarse grained **k**-point mesh. The short range part is Fourier transformed to real space and then recalculated easily by inverse Fourier transformation for a finer **k**-point mesh suitable to calculate the density of states. The long-range part arising from the electrostatic forces is added via an analytical expression. This approach is the same as the one described by Bungaro *et al.*[17] The calculation of the

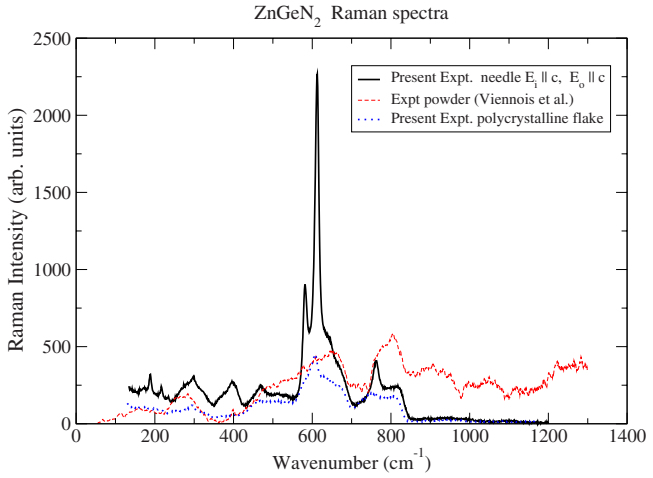


FIG. 3. (Color online) Comparison of the Raman spectrum measured for a needle-shaped single crystal with incoming and scattered light both polarized along the needle axis (black solid line), a polycrystalline flake (blue dotted line), and the published spectrum (red dashed line) for polycrystalline powders from Viennois *et al.* (Ref. 2). An arbitrary scale factor and offset was used to compare the spectra.

Raman tensor requires the calculation of a third rank tensor $\partial\chi_{\alpha\beta}/\partial\tau_{\kappa\gamma}$, where the susceptibility is a second derivative of the total energy versus two electric field components. Thus, it requires third derivatives of the total energy. This can still be achieved using only first-order changes of the wave functions using the $2n+1$ theorem,[18–20] as was described by Deinzer and Strauch[21] and Veithen *et al.*[7] and implemented in the ABINIT code.

## V. RESULTS

### A. Single crystal compared to polycrystalline experimental spectra

In Fig. 3, we show a typical experimental spectrum measured on a single crystal with incoming and scattered light both polarized along the long axis of the crystal (i.e., the $c$ axis) at normal incidence to one of the facets of the crystal as the solid line. The scattering geometry is thus either $x(zz)\bar{x}$ or $y(zz)\bar{y}$. This spectrum is compared to the spectrum published in the literature for polycrystalline powders[2] as well as with our own measurements of a polycrystalline spectrum. The differences between the present spectra and the previously published spectrum are striking. First, we see no evidence of spectral intensity above 850 $cm^{-1}$ even in our polycrystalline sample. These peaks were previously assigned tentatively to second harmonics. Second, the single crystal is now dominated by a strong and sharp peak near 612 $cm^{-1}$. Several other sharp features (e.g., at 582 $cm^{-1}$) are present that are absent in the powder spectra. This result indicates superior crystalline quality of our material and the importance of using polarized light to unravel specific modes.

### B. Calculated spectra

We show the calculated spectra for different symmetries in Fig. 4. It is noteworthy that the $a_{1t}$ spectra are about an order of magnitude stronger than the other spectra. Furthermore, although the peaks are at the same wave numbers, significant differences occur in the peak heights for different tensor components of the $a_{1t}$ Raman spectrum. Finally, the spectra for the different symmetries have peaks in quite different positions.

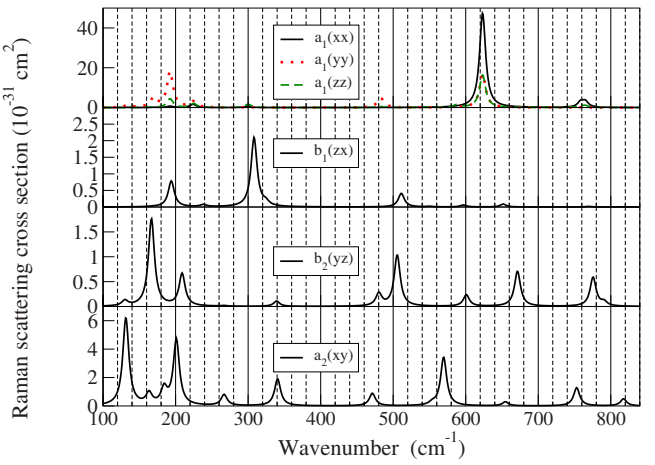


FIG. 4. (Color online) Calculated Raman intensities for different modes and Raman tensor components. Top panel: black solid ($xx$), red dotted ($yy$), and green dashed ($zz$)

### C. Comparison of theory and experiment for $a_{zz}^{1t}$

We begin our comparison of the experimental and calculated spectra to the $a_{zz}^{1t}$ component, which is in principle measured for the geometry $x(zz)\bar{x}$ or $y(zz)\bar{y}$ in Fig. 5. First, we can see that all the sharp features in the theory are indeed present in the experimental spectrum. By comparison to the individual phonon modes given in Ref. 1, we can make the assignments given in Table III. The error bars on the experimental frequencies here are 2 $cm^{-1}$. The agreement in peak position with the experimental peaks is within approximately

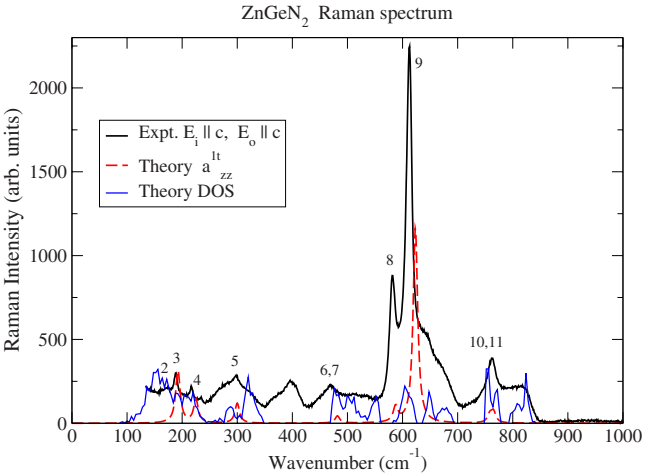


FIG. 5. (Color online) Comparison of experimental (thick solid black) and calculated spectrum for $a_{zz}^{1t}$ Raman tensor component (red dashed). Also shown is the phonon density of states (blue thin solid).

TABLE III. Phonon wave numbers of $a_{1t}$ modes (in $cm^{-1}$).

| Mode | Theor. | Expt. |
|---|---|---|
| 1 | 133 | |
| 2 | 168 | 170 |
| 3 | 192 | 187 |
| 4 | 224 | 215 |
| 5 | 300 | 297 |
| 6 | 483 | 467 |
| 7 | 485 | 467 |
| 8 | 586 | 582 |
| 9 | 623 | 612 |
| 10 | 760 | 762 |
| 11 | 764 | 762 |

5%. The mode number is indicated in Fig. 5. The calculated lowest frequency mode is too close to the elastic peak to be observed. The strongest peak is the mode occurring experimentally at 612 $cm^{-1}$. By inspecting the eigenvector of this mode, we can deduce that it has a wurtzite-$E_2^{high}$-like vibrational pattern. In the orthorhombic case, the motions in $x$, $y$, and $z$ directions are not strictly separated. The mode in question has both displacements in the $z$ direction and the $xy$ plane. However, it has opposite motions on corresponding atoms in the two layers of the crystal, characteristic of the $E_2$ symmetry. This mode corresponds primarily to a stretch of the various bonds lying in the basal plane layers. Similarly, the peak at about 582 $cm^{-1}$ can be labeled as a wurtzite-$A_1$-like mode. Again, it is not purely an $A_1$ mode, which would only have components in the $z$ direction, but it has the same direction of the motion in both layers, and there is a dominance of the stretching of the axial bonds in the $z$ direction. In both of these high frequency modes, the motion of the N atoms is much stronger than that of the Zn or Ge atoms. In wurtzite selection rules, only $A_{1t}$ should be visible in this geometry, $x(zz)\bar{x}$, but in orthorhombic selection rules, both correspond to the $a_{1t}$ and are thus allowed.

Next, we can see several additional broader features in the experimental spectrum. Most of these appear to correlate well with density of states (DOS) features, as shown in Fig. 5 by the blue thin solid line. For example, the high energy region has a plateau extending from about 750–850 $cm^{-1}$, which corresponds to four peaks in the DOS. The shoulders in the experimental spectrum at 640 and 670 $cm^{-1}$ correspond to the DOS peaks at 646 and 677 $cm^{-1}$. The DOS peak on the left of the main peak in the $a_{1t}$ spectrum is difficult to identify in the experimental spectrum because it overlaps with the 582 $cm^{-1}$ sharp peak. Between about 430 and 560 $cm^{-1}$, there is a plateau in the experimental spectrum that corresponds to three peaks in the DOS. On the left and right of the sharp feature identified as mode 5, we see a background that also corresponds to several peaks in DOS. Even in the low energy region, there is a background of DOS features.

The presence of vibrational DOS features in the spectrum indicates a relaxation of the momentum conservation rule. While the crystal size is too large to lead to appreciable relaxation of momentum conservation, the presence of defects such as stacking faults could also lead to a reduction in coherence length of the phonons. We have evidence from transmission electron microscopy[5] that stacking faults at a spacing of 10–20 nm are present in materials produced earlier.

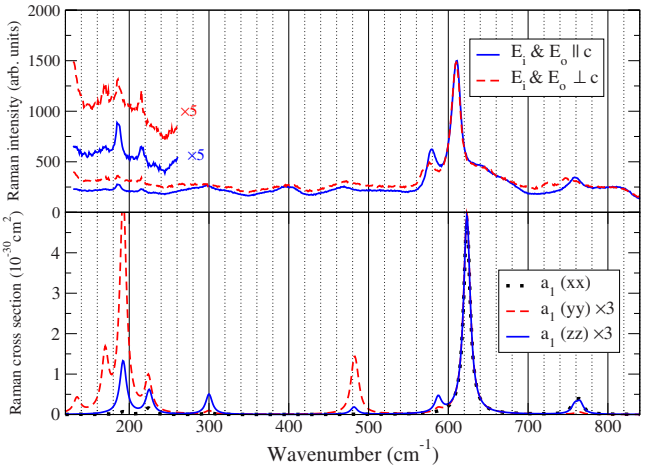


FIG. 6. (Color online) Polarization dependence of $a_{1t}$: top, experiment and bottom, theory. The line types and colors in experiment and theory match according to the discussion given in the text.

The only feature in the experiment which cannot be explained by any calculated feature thus far is the peak at 400 $cm^{-1}$. It was verified that this peak is not an artifact from the glass slide. We speculate that it could be some type of defect-localized vibrational mode.

### D. Polarization dependence of $a_{1t}$ modes

Next, we consider how the $a_{1t}$ spectrum depends on polarization. In Fig. 6, we compare the experimental spectra taken with polarizations parallel or perpendicular to the $c$ axis but with both input and scattered polarizations remaining parallel to each other. The spectra were renormalized to the peak height of the main peak. In the lower half of the figure, we show the different components of the calculated $a_{1t}$ spectrum. Note that the $a_{zz}^{1t}$ and $a_{yy}^{1t}$ components are multiplied by a factor of 3. The experimental spectrum for the polarizations along $c$ corresponds to $a_{zz}^{1t}$ and is thus drawn in matching line types and color (blue solid). Note that, as mentioned previously, we cannot determine by visual inspection of the sample whether the perpendicular polarization direction corresponds to $x$ or to $y$. One of the main differences between the experimental spectra for the two polarizations is difference in the ratio of the 582 $cm^{-1}$ peak relative to that of the 612 $cm^{-1}$ peak. This difference is indeed also observed in both the $xx$ and $yy$ components of the calculated Raman tensor, although the suppression of the lower wave number peak in the spectrum with polarization perpendicular to $c$ is stronger in the theory than in the experiment. For the $yy$ component, the theory also predicts a larger intensity for modes 6 and 7 near 480 $cm^{-1}$ and for modes[2–4] in the low frequency region. This also is the case in the experimental spectra. In particular, we see clearly three peaks in the $\mathbf{E} \perp \mathbf{c}$

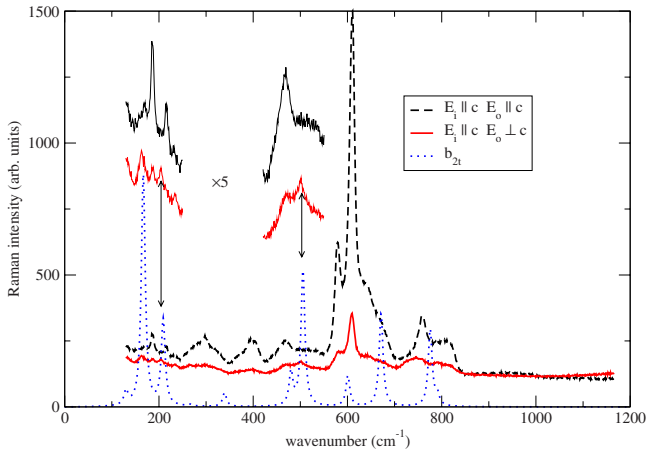


FIG. 7. (Color online) Raman spectra of $ZnGeN_2$ single for crossed polarizations. Both experimental spectra correspond to the input polarization parallel to $c$. The red solid line has the scattered light polarization perpendicular to $c$. The dashed black line has the scattered light polarization parallel to $c$ and is the same as shown in Fig. 5. The blue dotted line gives the calculated $b_{2t}$ spectrum.

spectrum near 200 $cm^{-1}$ instead of two, as shown by scaling up this region of the spectrum by a factor 5 in Fig. 6. The $xx$ component on the other hand would be weakened for these peaks. This result suggests that the measured spectrum corresponds more to $yy$ than the $xx$ component. We therefore display the $a_{yy}^{1t}$ spectrum in the theory and the $\mathbf{E}\perp\mathbf{c}$ experimental spectra in matching (red dashed) line types in Fig. 6. The observed differences in the 700–760 $cm^{-1}$ region are not as well reproduced by the calculation. However, we should remember that in this region, the experimental spectrum is strongly influenced by the "incoherent" DOS component. The theory predicts the $yy$ component to be suppressed relative to the $zz$ component in this range, whereby the DOS peaks would be more dominant.

We now consider the various ways in which a hexagonally faceted crystal can be lying on the glass slide. The facets can be either $(10\bar{1}0)$-like or $(11\bar{2}0)$-like and for each case either the short side of the hexagon or the long side of the hexagon could be the one lying on the plane. If the facet is $(10\bar{1}0)$, the longer side lies along $x$, and if this lies on the plane, it means the light comes in along $y$ and is $x$ polarized (if perpendicular to the $c$ axis). If the crystal is rotated by 60°, i.e., the short side lies in the plane, then one would measure $(a_{xx}^{1t}/4)+(3a_{yy}^{1t}/4)$. For the case of $(11\bar{2}0)$ facets, lying on the short side would mean that one measures purely $a_{yy}^{1t}$, while a rotated crystal lying on a long sided $(11\bar{2}0)$-like facet would mean one measures $(3a_{xx}^{1t}/4)+(a_{yy}^{1t}/4)$. Since we found above that the measured spectrum more closely resembles the $a_{yy}^{+}$ calculated spectrum, we can tentatively conclude that the sample had $(11\bar{2}0)$ facets and was lying on the shorter side of the hexagon. Although a mixture of $yy$ and $xx$ components cannot be completely excluded at this point, the next spectra taken with perpendicular polarizers (Fig. 7) confirm the $y$ orientation.

The observed polarization-induced differences are weaker than those predicted by the theory. This result may in part be due to the imperfect alignment of the polarizers and the finite solid angle of the incident and scattered light but also because of imperfect crystalline order, as discussed below.

### E. Crossed polarizations

In Fig. 7, we show (in red) the spectrum with crossed polarizers, i.e., input polarization along **c** and output polarization perpendicular to **c** measured on the same single crystal, which we have already tentatively determined to be oriented with its $y$ axis parallel to the glass slide. In principle, this geometry should measure the $b_{2t}$ spectrum, which is shown in the figure as the blue dotted line. For comparison, we also show the spectrum for both polarizers along $z$ in black. The calculations predict an entirely different spectrum of modes. In the experiment, however, we still see the same modes at 612 and 582 $cm^{-1}$, which dominated the previous spectra. Although these peaks have been strongly suppressed compared to the other polarization, they are still present in contrast to the calculation.

The presence of these peaks could in part arise from the imperfect alignment of the light polarization with the crystalline axes. We recall from Fig. 4 that the $a_{1t}$ spectrum is approximately 1 order of magnitude stronger than the $b_{2t}$ spectrum. If the alignment is off by an angle $\theta$ from the desired angle, we would mix in the wrong component proportional to $\sin^2\theta$, and we can make this error both in the input and in the output alignments. We are trying to see an order of magnitude smaller signal in comparison to the undesired one which could be mixed in by the misalignment. In practice, the alignment of the crystal relative to the polarizers can be made confidently to within about 2°. However, we also need to take into account that the input beam is focused through a lens on a small spot. In other words, not all the light is coming in normal to the surface. The half angle of the cone of light hitting the sample is estimated to be easily as large as 30°. Using the index of refraction of about 2.3,[1] we estimate that the light spreads within a cone of half angle of about 12° inside the material. This means that the input light polarization vector would be $\mathbf{e}_i=\cos\theta\hat{z}+\sin\theta\hat{x}$ assuming the plane of the light is perfectly aligned with the $xz$ plane. The output polarization would be $\mathbf{e}_o=\cos\theta\hat{y}+\sin\theta\hat{x}$. In that case, $\mathbf{e}_i\cdot\boldsymbol{\alpha}\cdot\mathbf{e}_o=\cos^2\theta\alpha_{zy}+\cos\theta\sin\theta(\alpha_{xz}+\alpha_{xy})+\sin^2\theta\alpha_{xx}$. So, we would mix in $b_{1t}$ corresponding to $xz$ and $a_2$ corresponding to $xy$ as well as the $a_{1t}$ $xx$ components in various degrees. The strong $a_{1t}$ component would ultimately come into the spectrum with a factor $\sin^4\theta$ factor which for 12° is about 0.002. So, even if this component is an order of magnitude stronger intrinsically, it should be smaller by at least an order of magnitude than the main component $b_{2t}$ we are trying to measure. This is obviously not the case. An alternative reason for why the $a_{1t}$ peaks are not that strongly suppressed will be discussed below.

Let us now first focus on whether we can see any evidence of the $b_{2t}$ spectrum at all. To do this, we consider the regions near 200 and 500 $cm^{-1}$ where peaks, characteristic of the $b_{2t}$ spectrum, are expected. For that reason, we include as insets a 5× blow up of these regions in both measured spectra. We may note that for the crossed polarizer spectrum,

there are three peaks in the region from 150 to 250 $cm^{-1}$, while for the parallel polarizers, there are two. The middle peak, which corresponds to the main peak in the $a_{1t}$ spectrum in this region, is indeed suppressed, and the outer peaks correspond well to the positions of the $b_{2t}$ calculated spectrum. So, we can tentatively assign the peak at 163 $cm^{-1}$ with the calculated mode $b_{2t}^2$ at 166 $cm^{-1}$ and the peak at 208 $cm^{-1}$ with the $b_{2t}^3$ mode. In the region near 500 $cm^{-1}$, we see evidence for the strong 506 $cm^{-1}$ $b_{2t}^7$ mode in the new experimental peak at 504 $cm^{-1}$. Identifying the higher predicted modes $b_{2t}^9$ at 673 $cm^{-1}$ and $b_{2t}^{10}$ at 775 $cm^{-1}$ is hindered by the presence of DOS features in these wave number ranges. Finally, we note that the spectrum shows no features which correspond to $b_{1t}$ (shown in Fig. 4) and thus confirms again the orientation of the crystal under study to be such that $y$ is parallel to the glass plate.

We return to the question as to why the main peaks are not as strongly suppressed by this polarization geometry as we would expect. One possible explanation for this is that the samples may not be perfectly ordered. In fact, as already mentioned, the ever-present strong peak at 612 $cm^{-1}$ corresponds to a mode with an $E_2$-type vibrational pattern if viewed as a wurtzite-type mode. In other words, it involves primarily motions in the $xy$ plane, which are opposite in phase between the two ($c$ direction) layers in the unit cell and involve primarily N-atom motions. This $E_2$ mode in the wurtzite selection rules should be visible both for perpendicular and parallel incoming and scattered light polarizers if both are in the $xy$ plane, as was mentioned at the end of Sec. III. In wurtzite, this mode should, however, not be visible for $y(zz)\bar{y}$ geometry because that geometry would only measure $A_1$. Both $E_2$ and $A_1$ are compatible with $a_1$ so using orthorhombic selection rules predicts the mode to be present and in fact quite strong. It thus appears that we are observing a superposition of a spectrum obeying the wurtzite and another spectrum obeying the orthorhombic selection rules. This result indicates that there is only partial ordering on the cation sublattice. Clearly, there must be some ordering; otherwise, we could not explain seeing all the multiple modes we identified in the $a_{1t}$ spectrum. On the other hand, the persistence of the main peaks at 612 and 582 $cm^{-1}$ in all spectra, which correspond to the strongest wurtzite $E_2$ and $A_1$ modes, indicates that this ordering of the cation sublattice is not perfect.

### F. Polycrystalline spectra

The samples produced by the present growth technique contain not only single crystal needles with dimensions, as described before but also polycrystalline regions. Some of these appear to be thin flakes and have occasionally hexagonal edges but no clearly defined hexagonal platelet crystals could be isolated. A Raman spectrum on these flakes was shown in Fig. 3. This spectrum showed no well-defined polarization dependence, which suggests a polycrystalline nature. The dome at the end of the needles was previously analyzed by electron diffraction to be polycrystalline.[5] A Raman spectrum on one of these domes is shown in Fig. 8 and compared with the spectrum on the flake. The spectrum shows considerably more background scattering and again

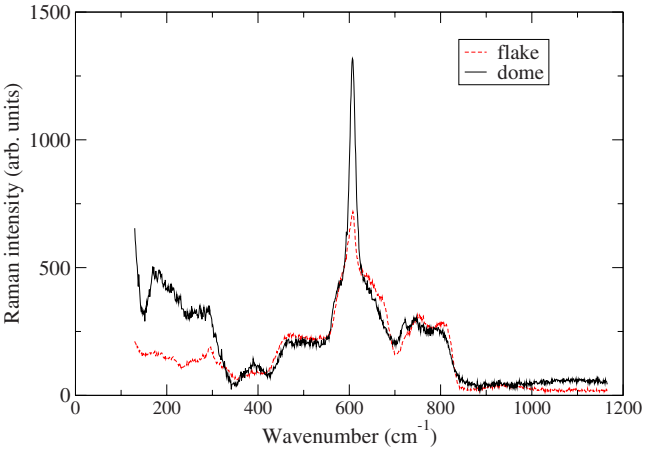


FIG. 8. (Color online) Raman spectra on two types of polycrystalline material: dome (solid black line) (after background subtraction) and flake (red dashed line).

essentially no polarization dependence except for the usual suppression if we use crossed polarizers. Both the dome and flake spectrum show similar features to the single crystal spectra except that the sharp peaks in the single crystal spectra become more rounded in the polycrystalline spectra. In other words, they are somewhat more DOS-like but the main peak near 612 $cm^{-1}$ is still present to varying degrees. In fact, this peak appears stronger in the dome than in the flake spectra. Also notable but at this moment unexplained is the fact that the peak at 400 $cm^{-1}$ is more suppressed in the polycrystalline spectra for the flake. No indication of harmonics above 850 $cm^{-1}$, as found in the previously published powder spectra is found here.[2] This difference may be related to the size of the crystallites in the previous work, on which, however, no information was provided by those authors.

## VI. CONCLUSIONS

A micro-Raman study of the vibrational modes in $ZnGeN_2$ single crystals and polycrystalline material was presented. The spectra obtained are very different from the previously reported spectra on powders, notably by the absence of any peaks above 850 $cm^{-1}$. Those features were previously identified as two-phonon or second order Raman features.[1]

For the $a_1$ symmetry spectrum on single crystals, which was theoretically predicted to be the dominant component, it was possible to identify ten of the 11 individual modes by a direct comparison between theory and experiment. Agreement in peak positions is within a few percent. This result indicates high quality of the crystallite and ordering of the Zn and Ge atoms on the cation sublattice leading to the orthorhombic symmetry selection rules. Additional features in the spectrum could primarily be identified with the vibrational DOS peaks and thus indicate the partial relaxation of the momentum conservation rule due to a reduced phonon coherence length. The latter is likely due to the presence of lattice defects.[5]

The polarization dependence of the measured spectra was much weaker than predicted by the theory. Nevertheless, the analysis of the polarization-induced changes allowed us to determine the orientation of the crystal relative to the glass slide and to identify a few of the $b_{2t}$ modes and the differences between the $a_{zz}^{1t}$ and $a_{yy}^{1t}$ components of the Raman tensor in the experimental spectra. The presence of the strongest $a_{1t}$ modes in geometries, in which it should be absent, cannot be accounted for solely by the large aperture angle. The main peak at 612 $cm^{-1}$ was found to have a wurtzite $E_2$-high-like vibrational pattern and is expected to be allowed using the wurtzite selection rules for both parallel and crossed polarizers. This observation suggests that the spectrum can be viewed as a superposition of a spectrum following orthorhombic and a spectrum following wurtzite selection rules, which in turn indicates that the ordering of the cation sublattice is only partial. Finally, the spectra on two types of polycrystalline $ZnGeN_2$ material were also presented. Neither showed evidence of Raman excitation above 850 $cm^{-1}$, as had been reported previously for powders.[2]

## ACKNOWLEDGMENTS

This work was supported by the Air Force Office of Scientific Research under Grant No. F49620-03-1-0010, by the Army Research Office under Grant No. W911NF-06-1-0476, by the National Science Foundation under Grant No. DMR-0420765, and by the U.S. Department of Education under Grant No. P200A030186. The calculations were done using the CWRU-HPC cluster.

[1] W. R. L. Lambrecht, E. Alldredge, and K. Kim, Phys. Rev. B **72**, 155202 (2005).
[2] R. Viennois, T. Taliercio, V. Potin, A. Errebbahi, B. Gil, S. Charar, A. Haidoux, and J.-C. Tédenac, Mater. Sci. Eng., B **82**, 45 (2001).
[3] M. Wintenberger, M. Maunaye, and Y. Laurent, Mater. Res. Bull. **8**, 1049 (1973).
[4] M. Maunaye and J. Lang, Mater. Res. Bull. **5**, 793 (1970).
[5] K. Du, C. Bekele, C. C. Hayman, J. C. Angus, P. Pirouz, and K. Kash, J. Cryst. Growth **310**, 1057 (2008).
[6] Timothy J. Peshek, Shanling Wang, John C. Angus, and Kathleen Kash, in *Nitrides and Related Bulk Materials*, MRS Symposium Proceedings No. 1040E, edited by R. Kniep, F. J. DiSalvo, R. Riedel, Z. Fisk, and Y. Sugahara (Materials Research Society, Warrendale, PA, 2007), 1040–Q01–01.
[7] M. Veithen, X. Gonze, and P. Ghosez, Phys. Rev. B **71**, 125107 (2005).
[8] T. R. Paudel and W. R. L. Lambrecht, Phys. Rev. B **76**, 115205 (2007).
[9] P. Hohenberg and W. Kohn, Phys. Rev. **136**, B864 (1964).
[10] W. Kohn and L. J. Sham, Phys. Rev. **140**, A1133 (1965).
[11] J. P. Perdew and A. Zunger, Phys. Rev. B **23**, 5048 (1981).
[12] M. Fuchs and M. Scheffler, Comput. Phys. Commun. **119**, 67 (1999).
[13] X. Gonze, J. M. Beuken, R. Caracas, F. Detraux, M. Fuchs, G. M. Rignanese, M. Sindic, L. Verstraete, G. Zerah, and F. Jollet, Comput. Mater. Sci. **25**, 478 (2002)
[14] S. Baroni, P. Giannozzi, and A. Testa, Phys. Rev. Lett. **58**, 1861 (1987).
[15] X. Gonze, Phys. Rev. B **55**, 10337 (1997).
[16] X. Gonze and C. Lee, Phys. Rev. B **55**, 10355 (1997).
[17] C. Bungaro, K. Rapcewicz, and J. Bernholc, Phys. Rev. B **61**, 6720 (2000).
[18] X. Gonze and J.-P. Vigneron, Phys. Rev. B **39**, 13120 (1989).
[19] X. Gonze, Phys. Rev. A **52**, 1086 (1995).
[20] X. Gonze, Phys. Rev. A **52**, 1096 (1995).
[21] G. Deinzer and D. Strauch, Phys. Rev. B **66**, 100301(R) (2002).